ACS Biomaterials SCIENCE & ENGINEERING

pubs.acs.org/journal/abseba

Article

High-Strength and Durable Functionalized PMMA/MPS-SiO_2/CNF Nanocomposite for a Photocurable 3D-Printed Dental Material

Priyanka Chaudhary, Tsui-Yun Chung, Chieh-Ming Tsai, Wei-Fang Su, Yu-Ching Huang,* and Meng-Fang Lin*

Cite This: https://doi.org/10.1021/acsbiomaterials.6c00466

Read Online

ACCESS | Metrics & More | Article Recommendations | Supporting Information

ABSTRACT: This work reports the preparation of a fibrous nanocomposite based on a poly(methyl methacryl/SiO_2) nanocomposite and cellulose nanofiber (CNF) (PMECS) for a photocurable 3D-printed dental material. The PME-based resin was prepared by mixing methyl methacrylate (MMA), ethylene glycol dimethacrylate (EGDMA), and PMMA powder. Incorporation of acrylate functionalized SiO_2 nanoparticles and CNF nanofibers into the PMMA matrix further improved the mechanical performance of the composites. The photocuring process promoted rapid polymerization, minimized defects, and enhanced dimensional stability. The resin was fabricated into incisor-shaped artificial teeth using stereolithography (SLA). Mechanical evaluation by Vickers hardness testing (HV) revealed a substantial increase in hardness from the neat resin PME (36 ± 3.8 HV) and PME/CNF (PMEC, 45 ± 2.4 HV) to the optimized PMECS65 hybrid composite (126.11 ± 4.3 HV). Notably, the 3D-printed teeth exhibited the highest hardness value (195 ± 5.4 HV), attributed to their enhanced interconnected fibrous morphology. Cytotoxicity tests confirmed the biocompatibility of the composites. These findings demonstrate that the fibrous PMECS resin significantly enhances the long-term strength and reliability of 3D-printed prosthetic dental strategies, making it an ideal material for high-end restorative dentistry.

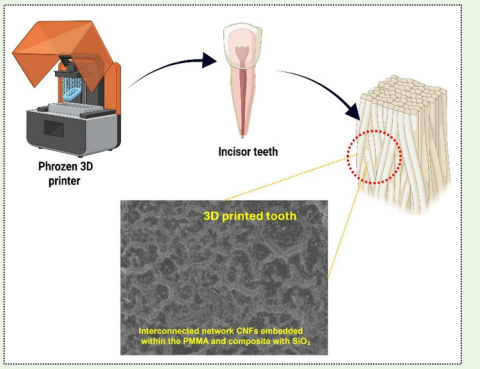

KEYWORDS: *dental biomaterials, additive manufacturing, fibrous scaffold, tissue engineering, PMMA, SiO_2*

INTRODUCTION

Additive manufacturing, commonly referred to as 3D printing, has been extensively used in the production of dental materials manufactured from metals, ceramics, and resins.[1] Among these, resin-based materials are gaining significant attention for applications such as artificial dentures, temporary crowns, wax patterns, and surgical implant guides.[2−3] Vat polymerization techniques, particularly stereolithography (SLA), are commonly employed in denture fabrication.[4] SLA 3D printing provides a rapid method to produce detailed forms with excellent precision and fidelity.[5−7]

A broad range of artificial denture teeth is commercially available, fabricated primarily from polymers. These polymers include conventional and modified acrylic resins, high cross-linked acrylic resins, and composite resins. Poly(methyl methacrylate) (PMMA) is a widely used polymer in dental practice, particularly for denture bases, provisional crowns, and occlusal appliances, because of its high aesthetics, clinical tolerability, and ease of processing. However, PMMA suffers from intrinsic drawbacks, including low fracture toughness, high susceptibility to wear and abrasion, polymerization shrinkage, and hydrolytic degradation, all of which compromise long-term reliability. These disadvantages are even more pronounced in digital dentistry, where 3D-printable and photocurable PMMA resins are increasingly employed. Early approaches to address these challenges involved PMMA nanocomposites. PMMA/SiO_2 nanocomposites improved hardness and thermal stability but suffered from nanoparticle agglomeration and poor dispersion within the matrix.[8] PMMA/ZrO_2 composites enhanced flexural strength and fracture toughness, but compromised translucency.[9] Similarly, PMMA/TiO_2[10] and PMMA/Al_2O_3[11] nanocomposites improved wear resistance and mechanical properties, yet particle clustering and poor optical properties limited their suitability for aesthetic restorations.[12−14] Silicon dioxide (SiO_2) nanoparticles remain particularly promising as fillers as they can improve hardness, modulus, wear resistance, and thermal stability while reducing shrinkage. Nevertheless, poor compatibility with the PMMA matrix, strong hydrogen bonding among surface silanols, and nonuniform dispersion frequently reduce translucency, increase viscosity, and impair

Received: March 18, 2026
Revised: May 15, 2026
Accepted: May 18, 2026

stress transfer across interfaces. Although silane coupling agents have been employed to mitigate these issues, incomplete functionalization often results in particle debonding, hydrolytic instability, and only modest mechanical improvement.

Consequently, conventional PMMA/SiO_2 composites provided only partial success, often sacrificing aesthetic and processing properties for mechanical reinforcement. More recently, functionalization of silicon dioxide with methacryloxy propyltrimethoxysilane (MPS) has proven more effective, enabling covalent anchoring of silicon dioxide within the PMMA matrix during photocuring. This strategy reduces agglomeration and preserves optical clarity. Parallel to inorganic fillers, fibrous reinforcement has been explored. Glass and polyethylene fibers improved flexural strength but negatively affected aesthetics and mechanical reliability.[15] By contrast, cellulose nanofibers (CNFs) have emerged as renewable, high-specific-strength reinforcements with a fibrillar architecture resembling dentin and periodontal tissues.[16] CNFs not only provide crack bridging, deflection, and pull-out toughening mechanisms but also create a fibrous microenvironment favorable for cell adhesion and migration, thus broadening the bifunctional scope of PMMA systems. However, previously developed PMMA/CNF composites were hindered by poor dispersion within hydrophobic matrices and limited compatibility with photocurable formulations, restricting their use in 3D-printed prosthetics.[17]

In this study, a photocurable fibrous PMMA composite incorporating MPS-modified silicon dioxide nanoparticles and CNF is proposed. The bonding at the interface of silicon dioxide is improved by MPS modification, which bonds PMMA and silicon dioxide covalently, thereby inhibiting agglomerate formation and providing stability over a prolonged period. The novelty of our material is related to the combination of MPS-modified SiO_2 nanoparticles and CNF in the photocurable PMMA matrix; however, such a combination has not yet been reported or studied in any prior research.[18−19] In contrast to other PMMA-based materials reinforced with either particles (PMMA/SiO_2) or fibers (PMMA/CNF), we have developed a composite with a unique architecture where both particulate and fibrous reinforcements can be used. The presence of MPS groups allows for the creation of bonds between SiO_2 nanoparticles and the PMMA matrix, while the addition of CNF results in an interconnected fibrous network, providing enhanced stress transfer and increased hardness. At the same time, CNF addition promotes mechanical strength with a fibrous structure, which acts as a biomimetic fibrous support facilitating cell migration. Through nanometer-scale interface modification and fibrous reinforcement at a multiscale level, this composite overcomes shortcomings such as filler agglomeration, brittleness, translucency, and poor bifunctionality in conventional PMMA composites.

■ MATERIALS AND METHODS

A 20–25 nm SiO_2 colloidal solution (MA-STM, 40 wt % solid content, Nissan Chemical Industries, Ltd.), 3-(trimethoxysilyl) propyl methacrylate (MPS, 98%, Acros Organics), polymethyl methacrylate (PMMA, Sigma-Aldrich Co. LLC, Darmstadt, Germany), methyl methacrylate (MMA, FujifilmWako Pure Chemical Corporation, Osaka, Japan), ethylene glycol dimethacrylate (EGDMA, FujifilmWako Pure Chemical Corp., Osaka, Japan), and phenyl-bis(2,4,6- trimethylbenzoyl) phosphine oxide (BAPO, Tokyo Chemical Industry Co., Ltd., Tokyo, Japan) were purchased and used as received, without further purification.

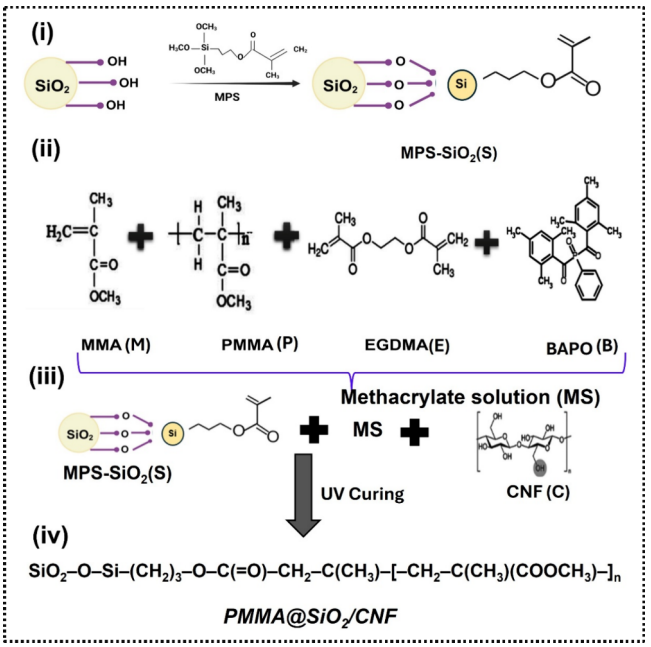

Figure 1. Preparation procedures of PMMA@SiO_2 /CNF. (i) Synthesis of MPS- SiO_2. (ii) Functionalization of PMMA. (iii) Mixing of MPS-SiO_2 into PMMA and CNF. (iv) UV-Curing to form nanocomposite PMECS.

Synthesis Method

The synthesis of the PMMA@SiO_2/CNF (PMECS) composite was completed through a four-step process, as illustrated in Figure 1(i–iv). This scheme outlines the hybrid reinforcement, surface modification, and polymerization strategy employed to fabricate the multiscale composite. The silicon dioxide modification was performed according to a previously reported procedure from our group.[20]

To prepare MPS-modified silicon dioxide, 12.5 g of an MA-ST-M SiO_2 colloidal solution was mixed with 20 g of methanol and stirred for 10 min. In the next step, 2.5 g of MPS was added, and the reaction was carried out at 50 °C for 24 h to achieve a solution of MPS-functionalized silicon dioxide nanoparticles. The PMMA-based resin was prepared by adding 30 wt % PMMA powder into a liquid mixture containing 14 wt % MMA and 56 wt % EGDMA monomers. The mixture was stirred magnetically at 300 rpm and 80 °C for 2 h. The resulting mixture was cooled to 25 °C, and the photoinitiator BAPO was added and stirred for 1 h, yielding the liquid resin shown in Figure S1. The PMECS composite was synthesized by a simple mixing process as described in the literature.[21] PMMA, functionalized SiO_2, and CNF were combined in a weight ratio of 3:1:0.2 at 45 °C and stirred for 6 h to prepare the printable ink. In the formulation, the functionalized SiO_2 concentration varied according to the experimental design, while the CNF content was maintained constant due to its fibrous and bundled morphology, as summarized in Table S1.

Characterization

The synthesized PMMA and all PMECS composites were confirmed using scanning electron microscopy (SEM; Hitachi, Model S-3400N) and Fourier-transform infrared (FTIR) spectroscopy (PerkinElmer-L160000W). Mechanical properties were evaluated by Vickers hardness testing (HMV-G series, Shimadzu), and wettability was assessed through contact angle measurement. Detailed methods of sample

https://doi.org/10.1021/acsbiomaterials.6c00466
ACS Biomater. Sci. Eng. XXXX, XXX, XXX–XXX

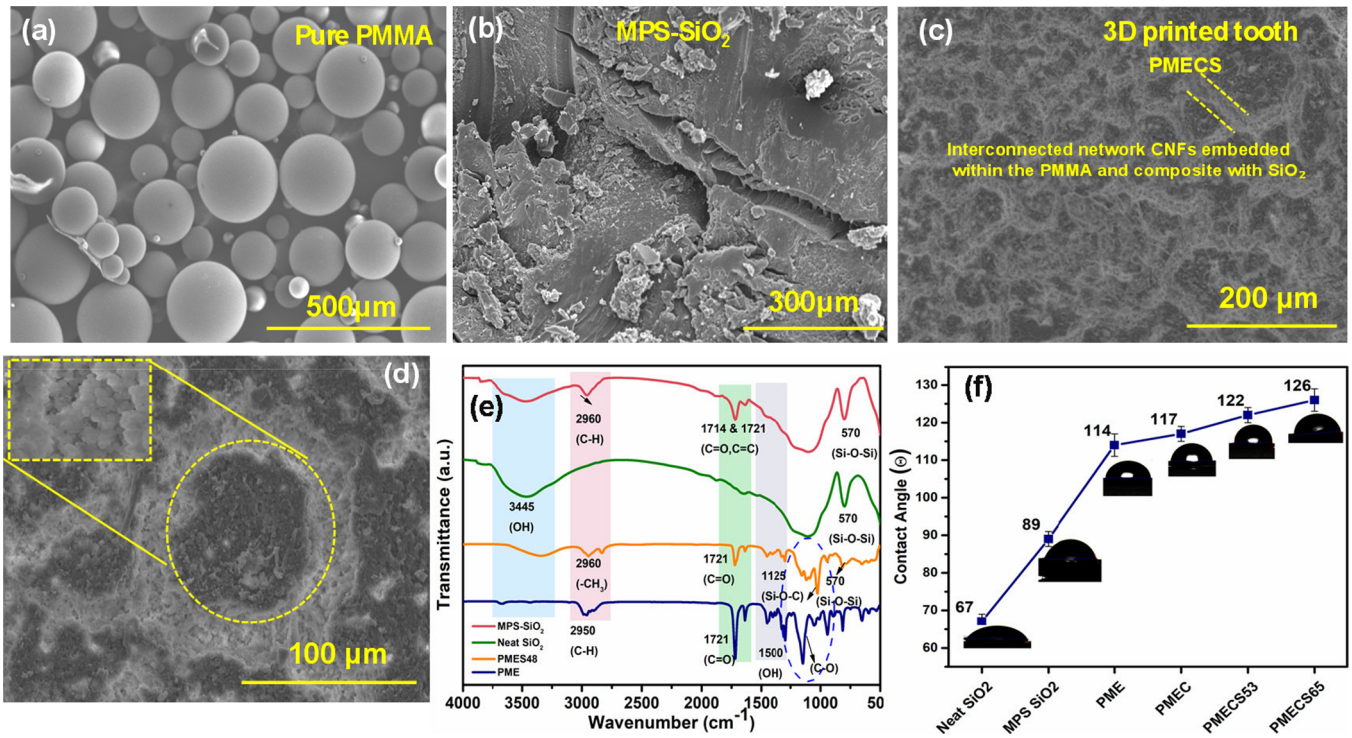

Figure 2. Characteristics of the raw material and the composite. (a) PMMA powder. (b) MPS-SiO_2. (c,d) 3D-printed tooth (composite) at 200 and 100 µm. (e) FTIR analysis of the composite. (f) Wettability test for hydrophobicity.

preparation and the information on the instruments used for each analysis are provided in the Supporting information, sections S1.1– S1.4.

■ RESULTS AND DISCUSSION

Figure 1(i–iv) shows the synthesis of the materials from step to step, with each step representing a different stage of the mechanism. In step (i) of Figure 1, the silicon dioxide nanoparticles were functionalized with 3-(trimethoxysilyl)propyl methacrylate (MPS). The surface silanol groups present in each nanoparticle of SiO_2 react with the methoxy groups present in MPS, resulting in covalent bonding in the form of Si–O–Si interconnectivity and attaching the methacrylate functional groups to a silicon dioxide surface. The product of this step is a functionalized silicon dioxide nanoparticle named SiO_2-MPS, which can react with methacrylate monomers during a polymerization event. Step (ii) involved the mixing of organic components of the resin matrix. MMA and PMMA served as the primary monomers and prepolymer, respectively. They were copolymerized in combination with EGDMA as the crosslinker and BAPO as the photoinitiator. The functionalized SiO_2-MPS particles were added to the resin matrix CNFs and mixed well in step (iii). The CNFs provided fibrous reinforcement and crack-bridging mechanisms, while the MPS-functionalized silicon dioxide ensured chemical compatibility with the methacrylate matrix, thereby improving particle dispersion and interfacial adhesion. Finally, step (iv) resulted in the formation of the PMECS composite structure after UV-curing. The resulting material consisted of a PMMA matrix integrated with covalently anchored silicon dioxide nanoparticles via methacrylate (MPS) linkage of CNFs. Such a hybrid organic/inorganic morphology brings about increased mechanical strength, higher surface roughness, and possible hydrophobic properties because of its hierarchical composite structure.

Figure 2 shows the characterization analysis performed on the raw material and the composite. As can be noted in Figure 2a, PMMA microspheres show a smooth spherical morphology with uniformity in size up to 500 µm; such uniformity in sizing leads to good spreading of the microspheres and adequate photocuring, which in turn are necessary for high-resolution 3D printing of dental resins. As can be noted in Figure 2b, SiO_2 microspheres have a rough morphology with an aggregated cluster size. The presence of these hard sites in the polymer matrix leads to enhanced interfacial transfer of stress in addition to improved hardness and wear resistance, both of which are essential requirements in dental composites used inside the mouth. CNF addition can be noted with a homogenous interconnecting network in a PMMA/MPS-SiO_2 matrix in Figure 2c,d. Precisely, increasing the CNF content enhances the hardness due to improved network connectivity and formation of an interconnected fibrous structure, which facilitate effective load distribution. However, this enhancement is observed only up to an optimal concentration, beyond which CNF agglomeration may occur, leading to stress concentration points and a potential decline in mechanical performance. Similarly, increasing the SiO_2 loading contributes to higher stiffness and hardness through efficient stress transfer, which is enabled by strong interfacial bonding introduced by MPS functionalization. Besides providing enhanced mechanical reinforcement in addition to crack deflection/bridging in a homogenously distributed manner, this network also replicates a natural matrix/ dentin structure to improve cell adhesion and biocompatibility. As can be noted in higher-magnification images in Figure 2 at the 100 µm scale, surface morphology

https://doi.org/10.1021/acsbiomaterials.6c00466
ACS Biomater. Sci. Eng. XXXX, XXX, XXX–XXX

of a 3D-printed composite highlights CNF dispersion and a bilayer interface between PMMA and MPS-SiO_2. Insertion highlights the nanostructure, which otherwise can aid in improving hydrophobicity. Other characterization examinations indicated the composition of the composite. Energy-dispersive spectroscopy analysis in Figure S2 confirms the purity of PMMA and the generation of a hybrid composite. Furthermore, comparisons presented in Figure S3a,d relate the pure PMMA morphology with composites, highlighting the effects of additives such as MPS-SiO_2 and CNF. This comparison demonstrates that the interconnected network is successfully locked and formed during the printing process, as evidenced by the post-printing SEM analysis. The morphological analysis verifies that CNFs are uniformly distributed and incorporated into the PMMA matrix together with MPS-modified SiO_2. Specifically, the SEM results show that CNFs are well-dispersed and embedded within the PMMA matrix along with MPS-functionalized SiO_2, forming a continuous network structure. These observations provide direct experimental evidence supporting the proposed network architecture in the printed composite. The surface functional groups of neat SiO_2, MPS-SiO_2, PME, and PMES48 were analyzed by FTIR spectroscopy. The characteristic absorption peaks of Si−O−Si were observed at 570 and 850 cm^{-1}, corresponding to bending and symmetric stretching vibrations, as shown in Figure 2e. The peak at 1120 cm^{-1} was assigned to asymmetric stretching vibrations of the SO−Si bond.[22] Further, the broad peak at 3445 cm^{-1} indicated hydroxyl (−OH) stretching vibrations from surface silanol groups, which interact with the silane group of MPS. After the surface modification, new peaks appeared at 1721, 1125, and 950 cm^{-1} for MPS-SiO_2 corresponding to C=C stretching, C−O stretching, and Si−O−C stretching vibrations of MPS, respectively. The reduction of the hydroxyl peak at 3445 cm^{-1} further confirmed the successful grafting of MPS onto the SiO_2 surface and displacement of surface hydroxyl groups. Analysis of the PMMA spectra indicates that the preferred band at 1724 cm^{-1} is a consequence of the stretching vibration of C=O, responsible for the ester functional group (−COO−). This band is strong and sharp, providing a guide for PMMA identification. The carbonyl linkage ester is especially critical in many polymers, above all in PMMA. In addition, between the 1125 cm^{-1} series of peaks, stretching vibrations of C−O−C along the ester linkage in PMMA are mostly responsible for these absorptions. This spectral area is typically used for detecting the presence of ester functional groups, which are vital to the PMMA structure, as they join methyl acrylate units in a chain.[23] The spectra from around 2950 cm^{-1} can be assigned to the stretching vibration of the C–H bonds of the methyl ($-CH_3$) groups attached to the PMMA backbone. Occasionally, a weak band might appear in the 1625 cm^{-1} region, most likely due to C=C stretching. Precisely, this band would rarely be associated with the C=C functional group for completely polymerized PMMA; instead, it may occur again due to the unconverted MMA monomer or residual impurities. FTIR analysis confirms the successful grafting of MPS onto SiO_2 nanoparticles, as indicated by the presence of characteristic methacrylate functional groups, which are capable of co-polymerizing with the PMMA matrix. This chemical functionality is expected to promote covalent linkage at the filler−matrix interface during photocuring. In addition to spectroscopic confirmation, the observed enhancement in mechanical properties, particularly the significant increase in Vickers hardness, provides strong indirect evidence of improved interfacial adhesion. From a mechanistic perspective, effective stress transfer in particulate-reinforced polymer systems is highly dependent on interfacial bonding; poorly bonded fillers typically act as defects, leading to stress concentration and reduced mechanical performance. In contrast, the consistent improvement in hardness observed in our system suggests efficient load transfer, which is indicative of improved interfacial compatibility and reduced interfacial slippage. Furthermore, it is well established in the literature that silane coupling agents such as MPS reduce surface energy mismatch, improve nanoparticle dispersion, and minimize aggregation, thereby enhancing the effective interfacial area. This improved dispersion, combined with covalent linkage, also contributes to restricting polymer chain mobility near the interface, resulting in increased stiffness and hardness. Additionally, stronger interfacial anchoring is theoretically known to reduce the likelihood of filler detachment and leaching under service conditions. In the spectra shown in Figure 2e, one observes the presence of a peak at 1724 cm^{-1} for PMES, stemming from the stretching vibration of the carbonyl groups in PMMA. The peaks observed at 1500 and 1350 cm^{-1} correspond to the –CH stretching modes of PMMA, with the peak at 1454 cm^{-1} being ascribed to methyl (CH_3) and that at 1392 cm^{-1} associated with methylene (CH_2). Further, upon the addition of MPS-SiO_2 nanoparticles, all PMMA/MPS-SiO_2 composites exhibit a very distinct peak at 1125 cm−1, characterized by the Si−O−Si bond, which evidently reveals the successful integration of SiO_2. Collectively, the FTIR spectra validate that the composite possesses the mechanical reinforcement, structural integrity, and aesthetic qualities required for artificial teeth, positioning it as a strong candidate for next-generation dental prosthetics that are durable, biocompatible, and visually natural.

The contact angle measurements for various concentrations of SiO_2 nanoparticles incorporated into PMMA are presented in Figure 2f. The control group of PME without SiO_2 demonstrated a contact angle of (114 ± 3°), indicating a hydrophobic nature. However, neat SiO_2 exhibits a hydrophilic nature (67 ± 2°) and MPS-SiO_2 shows a hydrophobic nature (89 ± 2°). With the addition of MPS-SiO_2, there was a significant increase in the contact angle, suggesting enhanced hydrophobicity. The performance and behavior of 3D photocuring printing depend heavily on the hydrophobic characteristics of their resin materials. The wettability of surfaces evaluated through contact angles determines the final surface properties and affects polymerization kinetics, layer adhesion, and print resolution in photocurable resin systems including PMMA and PMEC composite-based ones. A more hydrophobic resin formulation (contact angle > 90°) will resist moisture absorption, which will lead to better dimensional stability, interlayer adhesion, and optical clarity during curing. The observed increase in hydrophobicity, with a contact angle of approximately 126°, can be advantageous for dental applications as it helps reduce water absorption and swelling, thereby improving dimensional stability in the oral environment. Additionally, enhanced hydrophobicity may contribute to greater resistance against bacterial adhesion and subsequent biofilm formation, which is critical for maintaining oral hygiene and long-term material performance. However, excessively high hydrophobicity could potentially affect adhesion to surrounding tissues or interfaces. Therefore, achieving an optimal balance between hydrophobicity and interfacial compatibility is essential. Dental material

https://doi.org/10.1021/acsbiomaterials.6c00466
ACS Biomater. Sci. Eng. XXXX, XXX, XXX−XXX

applications benefit from hydrophobic surfaces that prevent unwanted resin spreading during printing while enabling easier layer separation and enhanced resolution of fine details. However, if over-hydrophobicity is not properly controlled,[24] the excessive hydrophobic nature of the material can create problems with wetting new layers, which can lead to interfacial defects and adhesion loss between layers. The optimal performance of 3D-printed components requires achieving an appropriate balance in surface hydrophobicity to achieve maximum printability, curing efficiency, and functional performance. The all-composition contact angle measurement is shown in Table 1.

Figure 3a–c illustrates the bioinspired fabrication of fibrous structures that replicate the internal morphology of natural incisor teeth using a Phrozen 3D printer via photocuring. At the top of the figure, the process begins with the Phrozen 3D printer, which employs ultraviolet (UV) light to cure liquid photopolymer resin into solid layers. The printing strategy is designed to mimic the fibrous architecture of natural incisors, as shown in the upper middle and right sections. Incisor teeth serve as the bio-inspiration since they possess a unique hierarchical structure and excellent mechanical strength, primarily derived from their anisotropic fibrous microstructure. This natural design is emulated through advanced layer-by-layer 3D printing. In Figure 3a, the schematic presents a cross-section view of the photocuring process, illustrating the formation of each new layer during printing. Figure 3b depicts the sequential photocuring mechanism. UV light is projected upward to selectively cure the resin and form the initial layer. Afterward, the build platform incrementally moves upward for successive curing cycles. This repetitive process results in the controlled fabrication of complex fibrous structures.[25]

Figure 3c shows the final printed product exhibits a well-defined, interconnected fibrous network that closely resembles the natural structure of incisor teeth. By accurately controlling the resin flow and localized curing, the process reproduces the anisotropic architecture responsible for the mechanical performance of biological tissues. Overall, this mechanism demonstrates how photocuring-based 3D printing enables the creation of biomimetic fibrous architectures with promising applications in dental restorations and tissue engineering.[25]

The final product is a printed item with a controlled fibrous network, similar to that of natural incisor teeth. By controlling the flow of resin and the curing of each layer with precision, the process enables reproduction of the anisotropic, fibrous structure that is the source of the mechanical behavior of biological tissues. This figure can demonstrate how 3D printing can be used to produce biomimetic structures having potential in dental or tissue engineering.

Figure 4a–d summarizes the mechanical property performance of different PMMA-based materials and the 3D-printed dental composites. The Vickers hardness test is one of the most popular methods for the testing of materials, especially for metals, ceramics, and polymers. The PME, PMEC, PMECS48, PMECS53, PMECS56, PMECS60, PMECS62, PMECS65, and a 3D-printed tooth were evaluated for mechanical performance. The PME (pure PMMA) case represents the lowest hardness, followed by PMEC (PMMA with CNF) and a relatively slow increment. Samples PMECS 48–65 are PMMA/CNFs with different MPS-SiO_2 nanoparticle contents (48–65 means weight % of MPS-SiO_2). The maximum

Table 1. Hydrophobicity of the Prepared Compositions[a]

material	contact angle (θ)
neat SiO_2	67 ± 2°
MPS SiO_2	89 ± 2°
PME	114 ± 3°
PMEC	117 ± 2°
PMECS53	122 ± 2°
PMECS65	126 ± 3°

[a]PME= PMMA [P] + MMA [M] + EGDMA [E]; PMECS =PMMA [P] + MMA [M] + EGDMA [E] +CNF [C] + SiO2 [S].

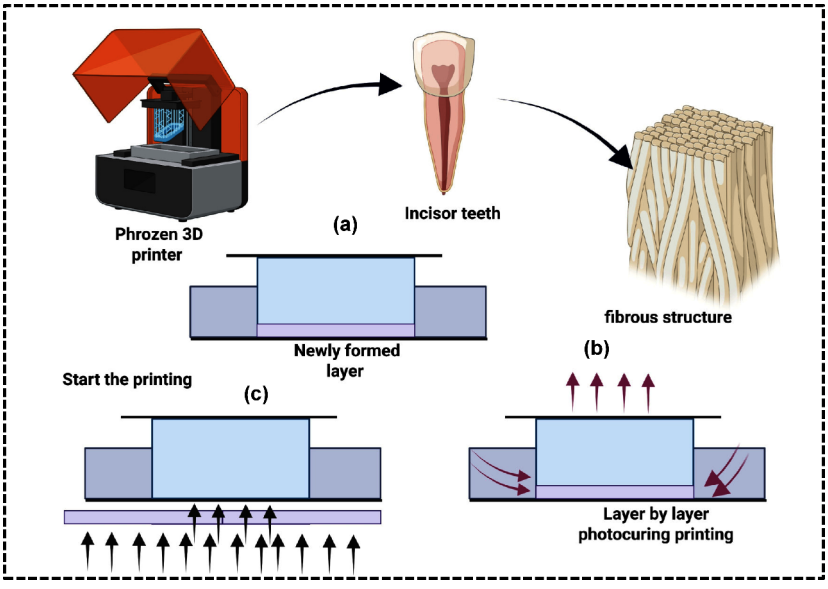

Figure 3. Illustration of the 3D-printing process formation: (a) newly deposited layer, (b) sequential layer-by-layer fabrication, and (c) stratified printing to construct the desired geometry.

https://doi.org/10.1021/acsbiomaterials.6c00466
ACS Biomater. Sci. Eng. XXXX, XXX, XXX–XXX

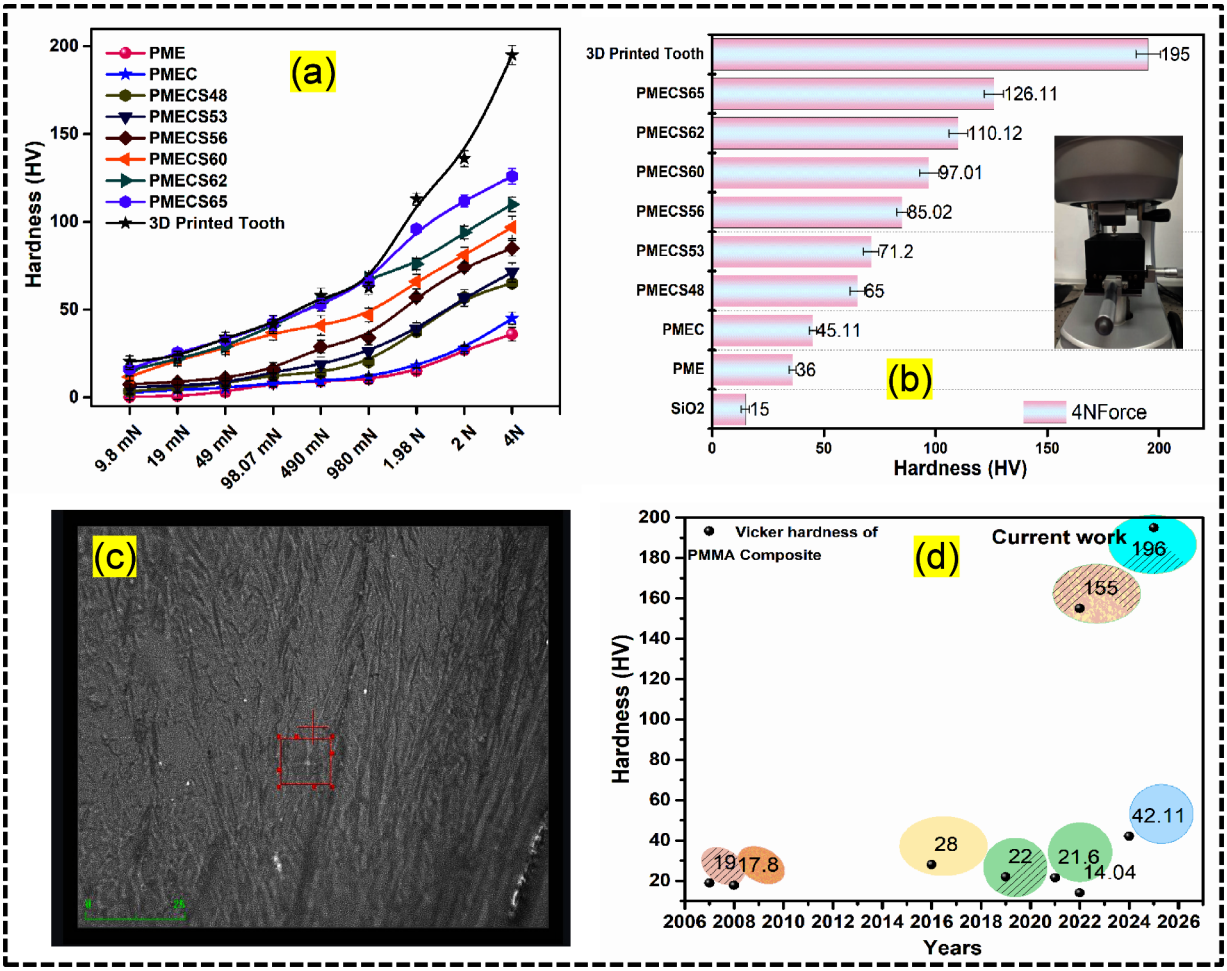

Figure 4. (a) Results of the Vickers test of samples at different forces. (b) Sample at 4 N force. (c) Digital photo of the material after the test. (d) Comparison of literature data with our composite PMECS 65.

hardness value under all loads is shown by the 3D-printed tooth (black star). The 3D-printed tooth exhibits better mechanical properties, particularly at higher loads (2 N, 4 N). This indicates that the enhancement of hardness by combining PMMA with CNFs and SiO_2 is synergistic. The inset figure in the curves is an optical micrograph or impression of indentation applied for the hardness test. The Vickers hardness (HV) values of all the specimens examined at various applied loads (9.8 mN~4 N) are shown in Figure 4a, and all composition hardness values are listed in Table S2. Hardness usually increases with a rise in force if the process flows remain constant. The 3D-printed tooth is harder at higher force values because of the mimic shape. Vickers microhardness measurements are routinely used to measure the hard characteristics of materials. The inset shows a microscopic sample area from where the data was obtained. In Figure 4b, only one bar represents the Vickers hardness (at a constant 4 N load) for comparison of different compositions of materials. The tooth sample exhibited a hardness of 195 HV; consequently, it is far greater than those of PME (36 ± 3.8), PMEC (45 ± 2.4), PMECS65 (126.11 ± 4.3), and neat SiO_2 (15 ± 2.1). The enhancement order clearly indicates that both CNFs and MPS-SiO_2 NPs enhance the mechanical properties. Figure 4c represents the diamond-shaped indentation during the Vickers analysis. The Vickers hardness data for PMMA composites collected from literature published during 2006–2025 are plotted in Figure 4d. Figure 4d represents a literature survey of previously reported PMMA-based composite materials and their mechanical properties (Vickers hardness, HV). The circle sizes were used for visual emphasis only and do not correspond to any quantitative parameter such as sample size or data weighting. The current data exhibit the highest mechanical strength (196 ± 5.4 HV), whereas the best previous value was 155 HV at much lower levels. The lowest hardness values reported for PMMA composites were below 50 HV. The incisor (front teeth) shape was used for printing with a width of approximately 6–9 mm and a height of around 10–12 mm, and the hardness measurement showed the highest value of HV.

The presence of continuous SiO_2 grains supports dental applications, hence preventing any apparent deformation of the PMMA matrix. The well-dispersed MPS-SiO_2 nanoparticles with a strong interface bonding to the PMMA lead directly to an increase in the proficiency of load transfer between the two formulations. The interfacial adhesion would further be enhanced owing to the MPS functionalization of SiO_2 surfaces, resulting in an increase in the general hardness of the composite. After MPS-SiO_2 and CNFs were added (PMECS56 to PMECS65), the hardness improved significantly compared to

https://doi.org/10.1021/acsbiomaterials.6c00466
ACS Biomater. Sci. Eng. XXXX, XXX, XXX–XXX

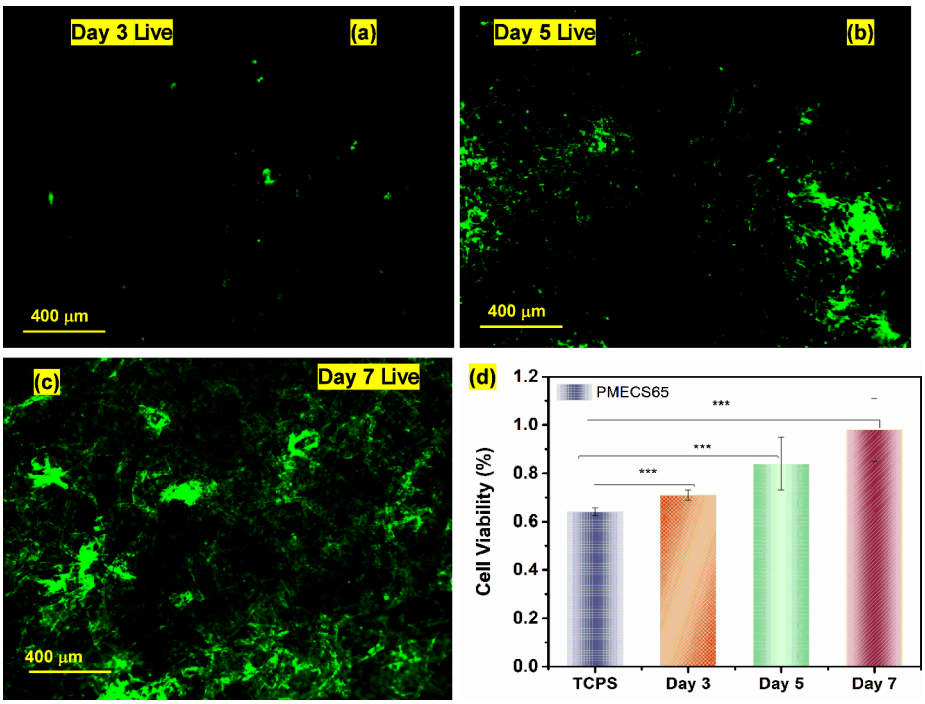

Figure 5. Cell growth study of the PMECS65 composite on (a) day 3, (b) day 5, and (c) day 7. (d) Cell viability study on days 3, 5, and 7, where $P < 0.001$.

that of natural dentin (60–90 VHN) and within values suitable for enamel-like applications. In the current work, the use of MPS-functionalized SiO_2 nanoparticles ensures covalent bonding with PMMA through the methacrylate groups. CNFs, on the other hand, interact with the polymer through hydrogen bonds and have a physical entangled fibrous network. It leads to increased interfacial interactions and efficient stress transfer. As a result, there is a synergistic effect wherein SiO_2 nanoparticles provide stiffness to the composite material and the CNFs allow efficient stress dissipation and formation of the entanglement network, leading to improved mechanical properties such as hardness. Acrylic-modified CNFs can indeed provide more active interaction with the polymer network and result in more covalent interaction. Therefore, the high content of the reactive CNFs and filler particles (both CNF and SiO_2) may result in excessive rigidness, leading to brittleness, making them unsuitable for use in dental applications due to mechanical loading in the mouth area. In our study, the optimal content of CNF and functionalized SiO_2 was found, ensuring a balance between hardness and flexibility. Currently, the observed hardness is higher, yet low enough not to become brittle. Thus, although modification of CNF by acrylic groups is a promising strategy, the use of such CNFs in dentistry will require additional optimization to avoid brittleness. The 3D-printed PMECS65 composite reaches 195 VHN, approaching the lower end of enamel hardness (270–360 VHN).[26] This indicates it is mechanically acceptable for occlusal surfaces, load-bearing dental prosthetics, or restorations.

The biocompatibility of the composite PMECS 65 was evaluated by cell growth and cell viability studies. Fluorescence live/dead imaging showed time-dependent increments of cell viability on the PMMA/MPS-SiO_2/CNF composite. Minimal cells were viable on day 3; cells grew into a fibrillar network on day 5. By day 7, almost confluent coverage of viable grown cells with sparse dead staining was observed on the composite, thus affirming extremely low. Qualitative findings were also supported by quantitative Alamar Blue assays; in total, the assays confirmed that, in addition to facilitating cell adhesion, the composite supports active long-term outgrowth and survival. The cell growth and cell viability studies of the PMECS65 composite on different days are depicted in Figure 5.

The live/dead assay results presented in Figure 5a–c demonstrate that after 7 days, the composite material PMECS65 exhibits excellent biocompatibility. The CNFs contribute a nanofibrous texture that exhibits a strong similarity to the extracellular matrix (ECM), providing a rich array of hydroxyl functions to enhance protein adsorption and integrin-mediated adhesion, thereby supporting cell attachment and migration. These qualitative observations were further validated by the quantitative Alamar Blue assay, as presented in Figure 5d. The cell viability from day 3 to day 7 depicted an abrupt rise, with values tending to rise well above what was observed for the standard TCPS control. The % increment from day 3 to day 7 was 71–97%, with the statistical analysis confirming time-dependent improvement in viability at "***$p < 0.001$", suggesting that the composite is biocompatible as well as favorable for long-term cellular growth. This further depicted that the PMECS 65 material not only allows cell survival but also promotes robust cell proliferation, highly desired for biomedical applications including tissue-engineering implants. The MPS-SiO_2 nanoparticles, being the main component in biomedical and dental composites, ensure silanol groups, enhancing surface wettability and promoting protein preconditioning layers that are quite essential for cellular interactions. Whenever silane coupling agents as MPS are incorporated, the interfacial bonding between SiO_2 and PMMA is favored, reducing filler leaching

https://doi.org/10.1021/acsbiomaterials.6c00466
ACS Biomater. Sci. Eng. XXXX, XXX, XXX–XXX

and promoting long-term biocompatibility. PMMA provides the structural integrity and optical clearness required for material usability, but its own hydrophobicity imposes a limitation on early-stage adhesion. The use of CNFs and MPS-SiO_2 improves the polymer's physicochemical characterization, producing a hybrid material that is stable, biocompatible, and supportive of cells. The PMECS65 composite, which achieved the highest Vickers hardness among the other composites, provides mechanically stable and durable microfracture under stress. Thus, PMECS65 is a promising material for dental and biomedical applications, where both load-bearing strength and cellular integration are crucial.

■ CONCLUSIONS

Photocurable PMECS composites reinforced with MPS-SiO_2 nanoparticles and CNFs were successfully synthesized. They are 3D printable and exhibited outstanding hardness and biocompatibility, along with having a fibrous microstructure that emulates the natural dental tissue architecture, imparting superior mechanical integrity. Furthermore, cytotoxicity tests confirmed that it possesses good biocompatibility to be used within dental environments. In conclusion, the synergetic effect of the reinforcement with MPS-SiO_2 and the fiber network formation within the resin material bestows outstanding strength, durability, and biocompatibility on this organic and inorganic fibrous composite, hence making it a promising candidate for artificial teeth and dental restorations.

■ ASSOCIATED CONTENT

Supporting Information

The Supporting Information is available free of charge at https://pubs.acs.org/doi/10.1021/acsbiomaterials.6c00466.

Experimental procedures and material details; formulation and synthesis of PMMA/MPS−SiO_2/CNF nanocomposites; photocuring and 3D-printing parameters; characterization techniques and instrumentation details; FTIR spectra analysis; SEM morphology images; mechanical property measurements; additional surface characterization results; and detailed discussion related to structural and mechanical performance (DOCX)

■ AUTHOR INFORMATION

Corresponding Authors

Yu-Ching Huang – *Department of Materials Engineering and Biochemical Technology R&D Center, Ming Chi University of Technology, New Taipei City 24301, Taiwan; Department of Chemical and Materials Engineering, Chang Gung University, Taoyuan 33302, Taiwan;* orcid.org/0000-0003-4772-8050; Email: huangyc@mail.mcut.edu.tw

Meng-Fang Lin – *Department of Materials Engineering and Biochemical Technology R&D Center, Ming Chi University of Technology, New Taipei City 24301, Taiwan;* orcid.org/0000-0002-9286-6527; Email: mflin@mail.mcut.edu.tw

Authors

Priyanka Chaudhary – *Department of Materials Engineering and Biochemical Technology R&D Center, Ming Chi University of Technology, New Taipei City 24301, Taiwan;* orcid.org/0000-0003-4841-0888

Tsui-Yun Chung – *Department of Materials Engineering and Biochemical Technology R&D Center, Ming Chi University of Technology, New Taipei City 24301, Taiwan*

Chieh-Ming Tsai – *Department of Materials Science and Engineering, National Taiwan University, Taipei 10617, Taiwan*

Wei-Fang Su – *Department of Materials Engineering and Biochemical Technology R&D Center, Ming Chi University of Technology, New Taipei City 24301, Taiwan; Department of Materials Science and Engineering, National Taiwan University, Taipei 10617, Taiwan;* orcid.org/0000-0002-3375-4664

Complete contact information is available at: https://pubs.acs.org/doi/10.1021/acsbiomaterials.6c00466

Author Contributions

P.C.: Data analysis, investigations, project administration, writing original draft, conceptualization. T.-Y.C.: Formal analysis. C.-M.T.: Visualization, validation. W.-F.S.: Validation, resources, editing. Y.-C.H.: Data curation, resource visualization. M.-F.L.: validation, supervision, resources, methodology, funding acquisition.

Notes

The authors declare no competing financial interest.

■ ACKNOWLEDGMENTS

The National Science and Technology Council (NSTC), Taiwan (NSTC 111-2221-131-019-MY3; NSTC 112-2628-E-131-001-MY4; NSTC 114−2221-E-131-038; NSTC 114-2221-E-131-012-MY3), financially supported this research. The authors would also like to sincerely acknowledge PHROZEN TECH CO., LTD and Mr. Yi-Jen Wu for their valuable technical support during 3D printing.

■ REFERENCES

(1) Muhammad, N.; Sarfraz, Z.; Zafar, M. S.; Liaqat, S.; Rahim, A.; Ahmad, P.; Alsubaie, A.; Almalki, A. S.; Khandaker, M. U. Characterization of various acrylate based artificial teeth for denture fabrication. *J. Mater. Sci. Mater. Med.* **2022**, *33* (2), 17.

(2) Jockusch, J.; Özcan, M. Additive manufacturing of dental polymers: An overview on processes, materials and applications. *Dent. Mater. J.* **2020**, *39* (3), 345–354.

(3) Tigmeanu, C. V.; Ardelean, L. C.; Rusu, L.-C.; Negrutiu, M.-L. Additive manufactured polymers in dentistry, current state-of-the-art and future perspectives-a review. *Polymers* **2022**, *14* (17), 3658.

(4) Li, W.; Xie, Q.; Wang, Y.; Sun, Y. Quantitative evaluation of edentulous maxillomandibular relationship record using diagnostic complete dentures fabricated by CAD and 3D printing. *J. Oral Sci.* **2022**, *64* (1), 59–62.

(5) Ali, I. L.; Yunus, N.; Abu-Hassan, M. I. Hardness, flexural strength, and flexural modulus comparisons of three differently cured denture base systems. *J. Prosthodont.* **2008**, *17* (7), 545–549.

(6) Ali Sabri, B.; Satgunam, M.; Abreeza, N.; N. Abed, A. A review on enhancements of PMMA denture base material with different nanofillers. *Cogent Eng.* **2021**, *8* (1), No. 1875968.

(7) Altarazi, A.; Haider, J.; Alhotan, A.; Silikas, N.; Devlin, H. Assessing the physical and mechanical properties of 3D printed acrylic material for denture base application. *Dent. Mater.* **2022**, *38* (12), 1841–1854.

(8) Kammona, N. R. K.; Radzi, Y. B.; Hameed, A. M. In Mechanical properties of PMMA reinforced with nano-SiO_2 for denture base

application, *AIP Conference Proceedings*; AIP Publishing LLC, **2025**; p 070005.
(9) Jamel, R. S.; Al-Murad, M. A.; Alkhalidi, E. F. The efficacy of reinforcement of glass fibers and ZrO_2 nanoparticles on the mechanical properties of autopolymerizing provisional restorations (PMMA). *Saudi Dent. J.* **2023**, *35* (6), 707–713.
(10) Alrahlah, A.; Fouad, H.; Hashem, M.; Niazy, A. A.; AlBadah, A. Titanium oxide (TiO_2)/polymethylmethacrylate (PMMA) denture base nanocomposites: mechanical, viscoelastic and antibacterial behavior. *Materials* **2018**, *11* (7), 1096.
(11) Roato, I.; Genova, T.; Duraccio, D.; Ruffinatti, F. A.; Zanin Venturini, D.; Di Maro, M.; Mosca Balma, A.; Pedraza, R.; Petrillo, S.; Chinigò, G. mechanical and biological characterization of PMMA/Al_2O_3 composites for dental implant abutments. *Polymers* **2023**, *15* (15), 3186.
(12) Radha, H. S. J.; Naji, S. A.; Haddad, A. I. Assessing Tensile and Shear Bond Strength between Artificial Acrylic Teeth and Nano-silica Reinforced PMMA Denture Base Material. *J. Nanostruct.* **2024**, *14* (1), 20–37.
(13) Choi, J. E.; Ng, T. E.; Leong, C. K.; Kim, H.; Li, P.; Waddell, J. N. Adhesive evaluation of three types of resilient denture liners bonded to heat-polymerized, autopolymerized, or CAD-CAM acrylic resin denture bases. *J. Prosthet. Dent.* **2018**, *120* (5), 699–705.
(14) Gad, M. M.; Fouda, S. M.; Al-Harbi, F. A.; Näpänkangas, R.; Raustia, A. PMMA denture base material enhancement: a review of fiber, filler, and nanofiller addition. *Int. J. Nanomed.* **2017**, *12*, 3801–3812.
(15) Somani, M. V.; Khandelwal, M.; Punia, V.; Sharma, V. The effect of incorporating various reinforcement materials on flexural strength and impact strength of polymethylmethacrylate: A meta-analysis. *J. Indian Prosthodont. Soc.* **2019**, *19* (2), 101–112.
(16) Kamble, V. D.; Parkhedkar, R. D.; Mowade, T. K. The effect of different fiber reinforcements on flexural strength of provisional restorative resins: an in-vitro study. *J. Adv. Prosthodont.* **2012**, *4* (1), 1–6.
(17) Kamble, V. D.; Parkhedkar, R. D. In vitro comparative evaluation of the effect of two different fiber reinforcements on the fracture toughness of provisional restorative resins. *Indian J. Dent. Res.* **2012**, *23* (2), 140–144.
(18) Hong, R.; Fu, H.; Zhang, Y.; Liu, L.; Wang, J.; Li, H.; Zheng, Y. Surface-modified silica nanoparticles for reinforcement of PMMA. *J. Appl. Polym. Sci.* **2007**, *105* (4), 2176–2184.
(19) Huang, J.; Chen, H.; Zhang, G.; Fan, X.; Liu, J. The Effect of Silane Coupling Agent on the Texture and Properties of In Situ Synthesized PI/SiO_2 Nanocomposite Film. *Nanomaterials* **2022**, *12* (2), 286.
(20) Lin, C.-C.; Hsu, S.-H.; Chang, Y.-L.; Su, W.-F. Transparent hydrophobic durable low moisture permeation poly (fluoroimide acrylate)/SiO_2 nanocomposite from solventless photocurable resin system. *J. Mater. Chem.* **2010**, *20* (15), 3084–3091.
(21) Hata, K.; Ikeda, H.; Nagamatsu, Y.; Masaki, C.; Hosokawa, R.; Shimizu, H. Development of dental poly (methyl methacrylate)-based resin for stereolithography additive manufacturing. *Polymers* **2021**, *13* (24), 4435.
(22) Lin, C.-K.; Xie, J.-W.; Tsai, P.-J.; Wang, H.-Y.; Lu, Z.-W.; Lin, T.-Y.; Kuo, C.-Y. The Effects of Different Blending Methods on the Thermal, Mechanical, and Optical Properties of PMMA/SiO_2 Composites. *J. Compos. Sci.* **2024**, *8* (9), 369.
(23) Zhang, Q.; Huang, W. X.; Zhong, G. J. Towards transparent PMMA/SiO_2 nanocomposites with promising scratch-resistance by manipulation of SiO_2 aggregation followed by in situ polymerization. *J. Appl. Polym. Sci.* **2017**, *134* (12).
(24) Saroia, J.; Wang, Y.; Wei, Q.; Lei, M.; Li, X.; Guo, Y.; Zhang, K. A review on 3D printed matrix polymer composites: its potential and future challenges. *Int. J. Adv. Manuf. Technol.* **2020**, *106*, 1695–1721.
(25) Bagheri, A.; Jin, J. Photopolymerization in 3D printing. *ACS Appl. Polym. Mater.* **2019**, *1* (4), 593–611.
(26) Craig, R. G.; Peyton, F. A. The microhardness of enamel and dentin. *J. Dent. Res.* **1958**, *37* (4), 661–668.

https://doi.org/10.1021/acsbiomaterials.6c00466
ACS Biomater. Sci. Eng. XXXX, XXX, XXX–XXX